Supporting Information

Scalable Binder-Free Supersonic Cold Spraying of Nanotextured Cupric Oxide (CuO) Films as Efficient Photocathodes

Jong Gun Lee,[a,†], Do-Yeon Kim,[a,†], Jong-Hyuk Lee,[a], Min-woo Kim[a], Seongpil An[a] Hong Seok Jo[a], Carlo Nervi[b], Salem S. Al-Deyab,[c] Mark T. Swihart[d], Sam S. Yoon[a,*]

[a]School of Mechanical Engineering, Korea University, Seoul 136-713, Republic of Korea

[b]Dept. of Chem, Univ. of Torino, Via P. Giuria 7, 10125, Torino, Italy and CIRCC (Bari)

[c]Petrochem. Research Chair, Dept. of Chem., King Saud Univ., Riyadh 11451, Saudi Arabia

[d]Dept. of Chem. & Biological Eng., University at Buffalo, The State University of New York, Buffalo, NY, 14260-4200, USA.

[*]**Corresponding author: skyoon@korea.ac.kr**

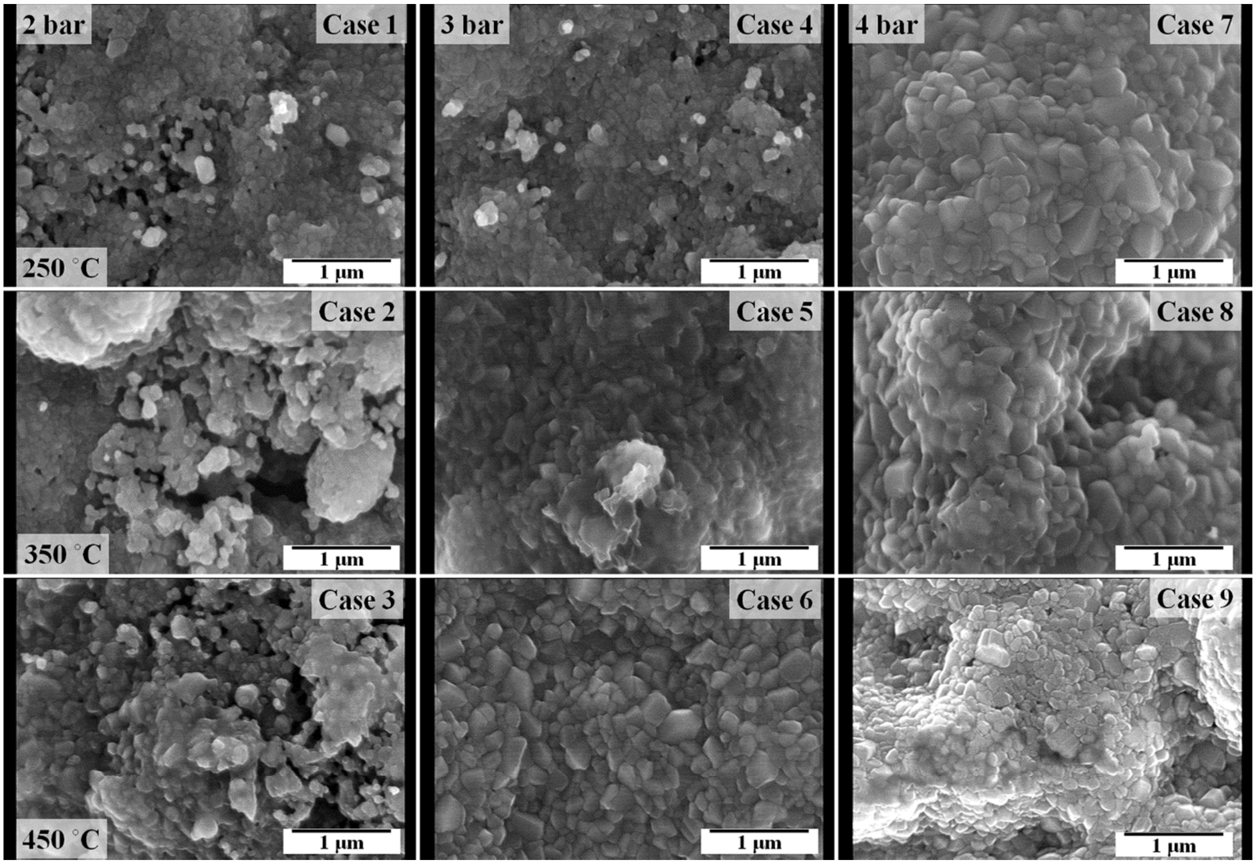

Figure S1. SEM images of cold-sprayed CuO films at various operating conditions. The gas temperature and pressure varied in the range 250 – 450 °C and 2 – 4 bar, respectively.

The surface morphology of the CuO films was also analyzed by AFM. **Figure S4** shows 3D AFM images for the cold-sprayed CuO films of Cases 1 – 9, which are summarized in **Table 3**. Case 1 exhibited the lowest roughness of 0.1 μm compared to other cases. For P_0 = 2 bar, it is apparent that Case 3 has the roughest surface morphology, which was not readily discernible from the corresponding SEM images in **Figure S1**. For P_0 = 3 bar, the change in roughness is not apparent in the AFM images; however, we qualitatively saw from **Figure S1** that the "dinosaur skin" texturing began to appear at T_0 = 450 °C, which is Case 6. For P_0 = 4 bar, the AFM images show that Case 9 has the roughest surface morphology. From the AFM images, we also see that the grain size increases with increasing impact velocity because the impact itself also has an *in* *situ* sintering effect. As discussed above, at these small grain sizes, grain growth is advantageous, although at larger grain sizes it eventually becomes undesirable.

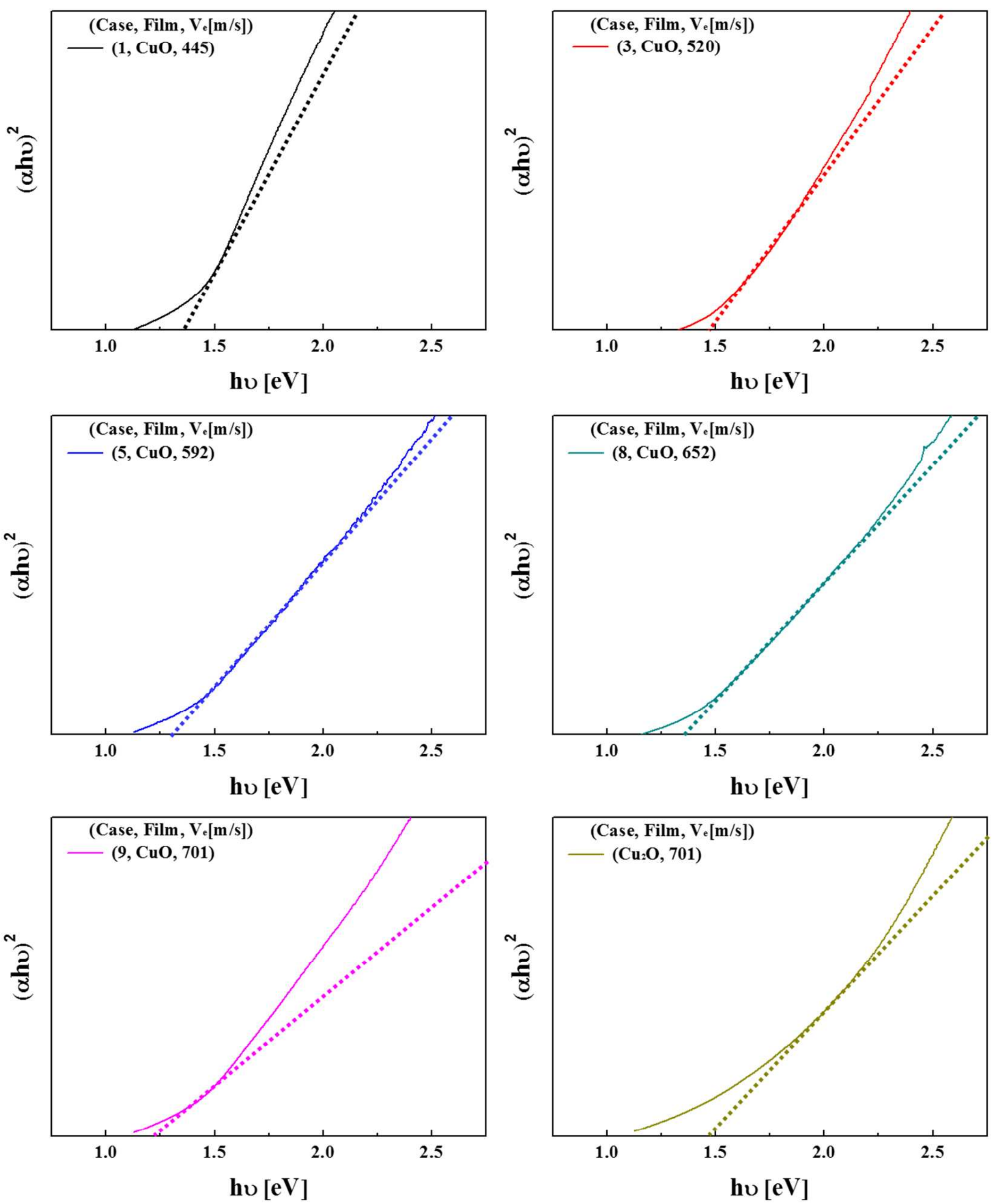

Figure S2. The effect of impact velocity on the bandgap of the CuO films. All films were annealed at 600 °C.

According to Kuczkowski[1], an optimal efficiency of 31% was found for sunlight conversion by a material with a bandgap between 1.1 and 1.4 eV. A bandgap outside this range could jeopardize the high efficiency of the sunlight conversion for any semi-conductor material. The bandgaps of our annealed CuO films were in the range of 1.0 – 1.3 eV, while that the bandgap of the as-deposited Cu_2O film was 1.33 eV, as noted in **Figure S2**. In order of decreasing impact velocity, Cases 9, 8, 5, 3, and 1 correspond to bandgap values of 1.08, 1.16, 1.19, 1.21, and 1.25 eV, respectively. Certainly, the bandgap decreased as the impact velocity increased, enabling a wider range of light to be received by the films. The as-deposited Cu_2O film had a bandgap of 1.33 eV and its photo-response was zero, not because of its bandgap, but because of its poor crystallinity, as previously mentioned.

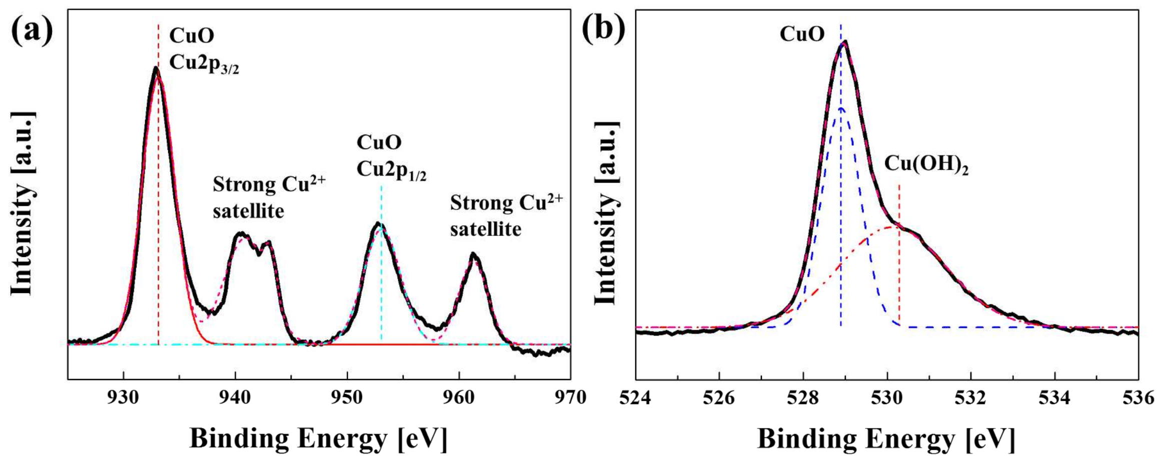

Figure S3. XPS spectrum of the CuO film annealed at 600 °C. (a) core level XPS of Cu 2p, (b)core level XPS of O 1s

The composition and chemical state of the elements of the CuO film annealed at 600 °C were investigated by XPS. **Figure S3a** shows the Cu 2p core-level region of the XPS spectrum, and a fit using Gaussian functions. The Cu 2p core-levels at 933.1 and 953.0 eV are attributed to Cu $2p_{3/2}$ and $2p_{1/2}$, respectively[2-3]. The gap between the Cu $2p_{3/2}$ and $2p_{1/2}$ levels is 20.0 eV, which is in agreement with the standard value for CuO [4-5]. In addition to the Cu $2p_{3/2}$ and $2p_{1/2}$ peaks, satellite peaks appear at binding energies of 942.9 and 961.2 eV, which is evidence of an open $3d^9$ shell corresponding to the Cu^{2+} state[6-7]. **Figure S3b** shows the XPS patterns of O 1s core level and fitting results with the Gaussian functions of the CuO film. The lower binding energy peak at 528.9 eV corresponds to oxygen in CuO, while the higher binding energy peak at 530.1 eV could arise from a hydroxyl species (*e.g.* $Cu(OH)_2$) due to adsorbed water from the atmosphere. The FWHM of the CuO binding energy is 1.2 eV, which has sharper binding energy peaks than $Cu(OH)_2$[8-9].

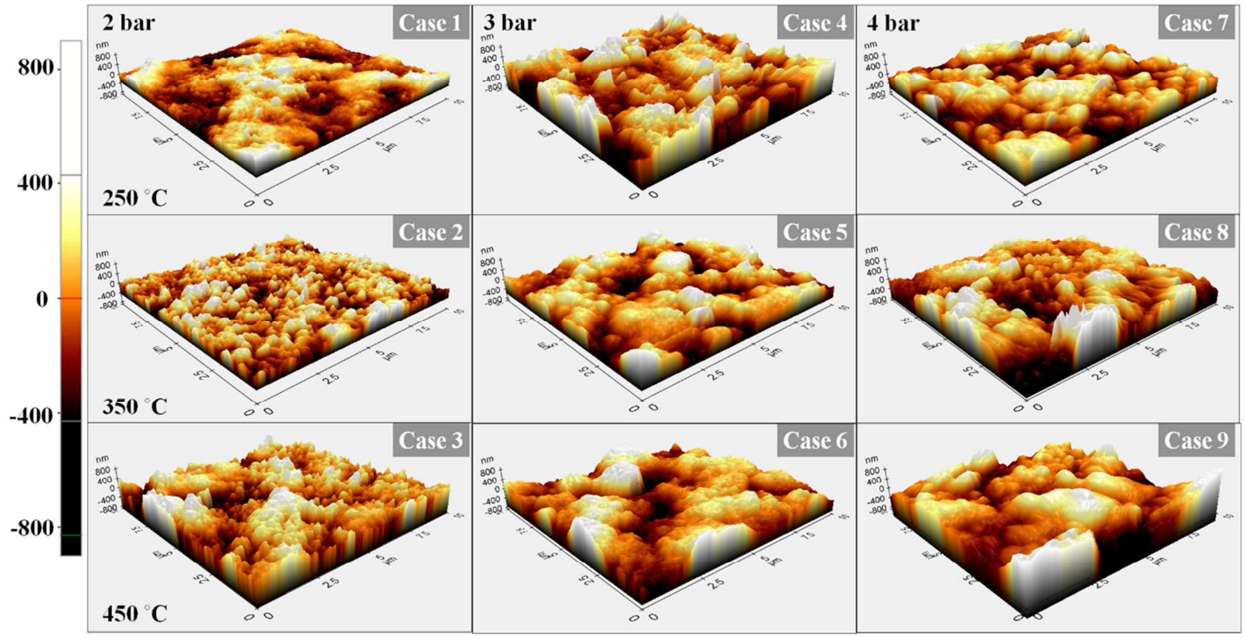

Figure S4. AFM images of the cold-sprayed CuO films at various operating conditions. The gas temperature and pressure varied in the range 250 – 450 °C and 2 – 4 bar, respectively.

References

1. Kuczkowski, A., Photoelectrochemical Processes at Semiconductors. *Photochem. Photophys.* **1990,** *3*, 103-136.
2. Wu, C.-K.; Yin, M.; O'Brien, S.; Koberstein, J. T., Quantitative Analysis of Copper Oxide Nanoparticle Composition and Structure by X-ray Photoelectron Spectroscopy. *Chem. Mater.* **2006,** *18*, 6054-6058.
3. Teo, J. J.; Chang, Y.; Zeng, H. C., Fabrications of Hollow Nanocubes of Cu_2O and Cu via Reductive Self-Assembly of CuO Nanocrystals. *Langmuir* **2006,** *22*, 7369-7377.
4. Zhu, J.; Chen, H.; Liu, H.; Yang, X.; Lu, L.; Wang, X., Needle-shaped Nanocrystalline CuO Prepared by Liquid Hydrolysis of $Cu(OAc)_2$. *Mater. Sci. Eng., A* **2004,** *384*, 172-176.
5. Lin, H.-H.; Wang, C.-Y.; Shih, H. C.; Chen, J.-M.; Hsieh, C.-T., Characterizing Well-ordered CuO Nanofibrils Synthesized through Gas-Solid Reactions. *J. Appl. Phys.* **2004,** *95*, 5889-5895.
6. Zhang, Z.; Wang, P., Highly Stable Copper Oxide Composite as An Effective Photocathode for Water Splitting via A Facile Electrochemical Synthesis Strategy. *J. Mater. Chem.* **2012,** *22*, 2456-2464.
7. Chusuei, C. C.; Brookshier, M.; Goodman, D., Correlation of Relative X-ray Photoelectron Spectroscopy Shake-up Intensity with CuO Particle Size. *Langmuir* **1999,** *15*, 2806-2808.
8. Wang, P.; Ng, Y. H.; Amal, R., Embedment of Anodized p-type Cu_2O Thin Films with CuO Nanowires for Improvement in Photoelectrochemical Stability. *Nanoscale* **2013,** *5*, 2952-2958.
9. Senthilkumar, V.; Kim, Y. S.; Chandrasekaran, S.; Rajagopalan, B.; Kim, E. J.; Chung, J. S., Comparative Supercapacitance Performance of CuO Nanostructures for Energy Storage Device Applications. *RSC Advances* **2015,** *5*, 20545-20553.